Reports

The Proton Microprobe: A Powerful Tool for Nondestructive Trace Element Analysis

Abstract. *A proton microprobe capable of focusing proton beams with energies up to 6 million electron volts to a spot size of 2 × 2 square micrometers has been used for chemical analysis of small grains of minerals in lunar samples by proton-induced x-ray emission. The proton microprobe is preferable to the electron microprobe for analyzing trace elements whose concentrations are below the detection limit of the latter and for analyzing objects with numerous major and trace elements with a wide range of atomic numbers. Application of the proton microprobe to biological samples is feasible.*

X-ray emission spectroscopy has been widely used for qualitative and quantitative determinations of trace elements in recent years. This is largely due to the rapid development of high-resolution Si(Li) detectors. The electron microprobe technique allows quantitative analysis of micrometer-sized particles, inclusions in solids, and biological samples. However, because of the high bremsstrahlung background from the electrons this method is limited to a sensitivity of 1 part in 10,000, so that only the major elements [with concentrations > 1000 parts per million (ppm)] in the sample can be quantitatively determined. To get information about elements with concentrations < 1000 ppm, one is forced to use other techniques such as x-ray fluorescence or neutron activation analysis. However, the last two methods are not applicable to microscopic objects. Trace elements in such small areas can be analyzed with the ion-probe (*1*) or laser mass spectrometer (*2*), but these techniques are destructive because material is sputtered from the sample surface. Nondestructive trace element analysis can be achieved by using a charged-particle beam of, for example, protons or alpha particles to induce the emission of characteristic x-rays of the elements present in the specimen (*3*).

The accelerators used are capable of producing beams of charged particles with energies and intensities that are continuously variable over a wide range. The beams can be tightly focused so that x-ray emission can be restriced to the small sample of interest (*4*). The penetration depth and the detection limits (*5*) can be chosen by varying the particle energy. It has been shown experimentally (*3*) that a combination of x-ray excitation by protons and detection of the emitted x-rays by an Si(Li) detector provides a powerful method for multielemental, nondestructive analysis of major and trace elements with atomic number $Z \geq 12$. Small concentrations of Ti (for example, 4×10^{-11} g) deposited on a thin carbon foil were easily detected by using a 1.5-MeV proton beam to induce the K x-ray emission spectra (*3*).

Until recently, the applicability of this technique to geological and biological problems was restricted because of experimental difficulties, such as collimating and focusing the ion beams to very tiny spots. In some respects the problem of spot size has been solved in different laboratories (*6, 7*). Wide application of the microbeam, however, depends on the reduction of the beam halo intensity—that is, the region outside the central spot. We tried to solve this problem and finally ended up with a 99.9 percent concentration of the beam intensity in an area of $2 \times 2\ \mu m^2$ (*4, 7*). The proton microprobe was built by a group of physicists from the Physikalisches Institut der Universität Heidelberg and the Max-Planck-Institut für Kernphysik, Heidelberg. The Heidelberg facility consists of two major parts: a collimator system (*7*) to produce the ion beam of micro dimensions and a focusing unit (Fig. 1). Figure 2 shows the experimental arrangement and the beam profile. The proton beam supplied by the 6-MV EN-Tandem Van de Graaff accelerator of the Max-Planck-Institut enters the collimator system through a hole 1 mm in diameter drilled in a thick, water-cooled brass plate. This plate decouples the accelerator vacuum from that of the collimator system and partly stops the portions of the beam that are not accepted by the collimator. The collimator consists of two pairs of crossed slits (called collimators 1 and 2) mounted in two chambers. The slits are made of stainless steel with highly polished sharp edges for optimal definition of the beam, as shown in Fig. 3. Several factors were taken into consideration in the selection of the angle and the dimensions of the slits.

1) Any particle hitting the entrance surface is stopped in the slit either because the scattering angle is less than θ_{in} ($\theta_{in} = 15°$) or because ions scattered into angles with $\theta \geq \theta_{in}$ are hitting the opposite slit. These ions can leave the slit only if they are scattered again into a large angle (11° to 19°), which is very unlikely.

2) For the exit surface an angle of $\theta_{out} = 4°$ was chosen in order to make the system insensitive to a divergence between beam direction and slit normal.

3) The distance of the beam-defining edge from the exit of the slit (4.8 mm)

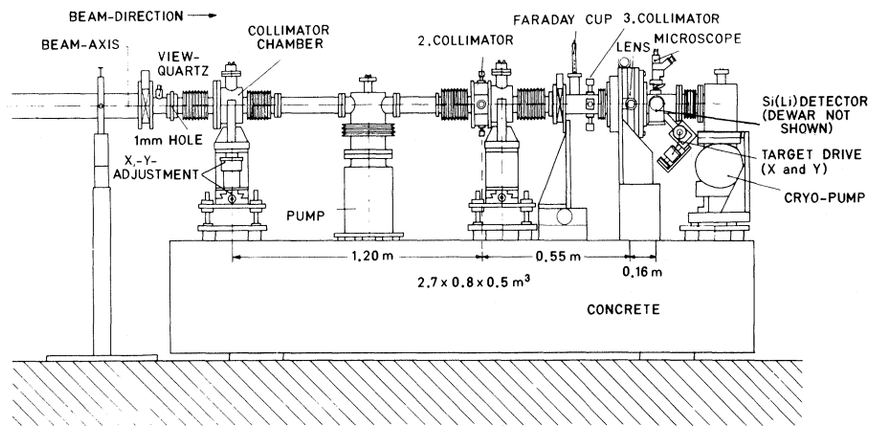

Fig. 1. Proton microprobe facility connected to the 6-MV EN-Tandem Van de Graaff accelerator of the Max-Planck-Institut für Kernphysik, Heidelberg.

0036-8075/78/0217-0765$01.00/0

was chosen to satisfy condition 1 for slit widths $d \approx 1$ mm.

4) An angle between the entrance and exit surfaces close to 180° is dictated by the required accuracy of the beam-defining edges. The roughness of the surfaces and the beam-defining edges was ≤ 0.1 μm. Moreover, the transparency of the edges should be smaller than the surface roughness. For the angles chosen the width of the transparency zone, as given by the range of 1-MeV protons, is 0.4 μm. But ions traversing this zone can only leave the slit if the average scattering angle is less than 4°. A root-mean-square angle of 4°, however, corresponds to values of the transparency zone much smaller than 0.1 μm. We thus conclude that scattered particles can only originate from a zone ≈ 0.1 μm wide, which is determined by the accuracy of the beam-defining edges of the slits.

As shown in Fig. 2, the first collimator has a slit width of $d_{1x} = 8$ μm and $d_{1y} = 45$ μm. The divergence of the transmitted beam is then reduced by means of a second collimator with $d_{2x} = 800$ μm and $d_{2y} = 500$ μm. The amount of protons scattered at the first and second collimators and transmitted by the antiscattering collimator can be estimated to be $< 10^{-4}$ I, where I denotes the intensity of the beam leaving collimator 1.

The collimated beam is then focused by a small magnetic quadrupole doublet onto the target (sample) located about 100 mm behind the second quadrupole. The quadrupoles are of a conventional type with air-cooled coils, an aperture diameter of 5 mm, an effective field length of 40 mm, and an outer yoke diameter of 170 mm. The guaranteed tolerances of the dimensions of the pole tips and the aperture diameter are $\pm$ 0.01 mm. A maximum field gradient of 500 tesla/m at 3 amp can be obtained, allowing one to focus protons or, for example, $^{16}O^{4+}$ ions with energies ≤ 25 MeV within 100 mm behind the second quadrupole. Thus, the lens is strong enough to permit its use with heavy-ion beams available from EN-Tandem accelerators. The beam can be adjusted during the experiment and a specific spot can be accurately selected by using an optical microscope fixed to the target chamber. This setup also permits simultaneous viewing of the sample during the experiment. The sample holder in the target chamber can be moved in both the x- and the y-direction by a step motor, allowing analyses of further areas without breaking the vacuum of the system.

Table 1. Composition of ilmenites and baddeleyite in lunar sample 75015 as measured with the electron microprobe at an excitation energy of 15 keV.

Component	Concentration (percent by weight) in		
	Ilmenite 3	Ilmenite 6	Baddeleyite
FeO	42.62	43.39	1.11
MgO	2.16	1.60	0.13
MnO	0.59	0.70	0.04
CaO	0.34	0.12	0.24
TiO_2	53.50	53.63	1.37
V_2O_3	ND*	ND	ND
Cr_2O_3	0.55	0.46	ND
Al_2O_3	0.42	0.35	0.55
SiO_2	0.06	0.11	0.20
ZrO_2	ND	ND	94.07
HfO_2	ND	ND	2.52
Totals	100.24	100.36	100.23

*ND, not detected.

The smallest proton beam achieved so far is 2×2 μm^2. Quantitative measurements of the beam profile showed an approximately rectangular intensity distribution (*4*). These measurements also led to an estimate of the halo of the beam: the ratio of the total beam intensity to the intensity measured outside the beam in a ring having a 20-μm inner diameter and a 1-mm outer diameter is of the order of 10^4. This high-quality focused ion beam is necessary for analyzing micrometer-sized objects in a sample. In most cases, however, this ratio of 10^4 to 1 is also sufficient with respect to the statistical accuracy that can be obtained in a reasonable measuring time ($\sim$ 2 to 3 hours). On the other hand, a beam halo with a higher or even an unknown intensity would introduce very strong uncertainties in the analyses.

The current density we obtained ranged from 5 to 20 pa/μm^2 at beam currents of 0.3 to 1 μa measured behind the analyzing magnet of the beam transport system. This density is sufficient to reach relative detection limits of the order of 1 to 10 ppm in a reasonable time for elements with $Z \geq 12$ even in small amounts of material with volumes of a few cubic micrometers and thicknesses of the order of the beam range.

Comparing the performance of the proton microprobe with that of other probes, especially the electron microprobe, we find the following advantages and limitations of the new technique. The main advantage of the proton microprobe is that its sensitivity is one or two orders of magnitude higher than that of the electron microprobe for detecting trace elements under normal operating conditions. Most of the problems and limitations of the proton microprobe arise from the relatively large penetration depth (20 to 70 μm) for protons with energies of 0.5 to 4 MeV, which has the following consequences.

1) For very thin samples the sensitivity is reduced because of the enhanced background (bremsstrahlung and characteristic x-rays) from the sample backing. This can be minimized in some cases by using a proper backing material (such as very pure carbon).

2) The x-ray yield changes with depth as the protons lose energy in the sample (*8*).

3) Fine-grained multicomponent targets are also excited from the areas just below the grain of interest, which thus obscures the results. In addition, quantitative evaluation of the x-ray spectra is difficult because of the influence of x-ray

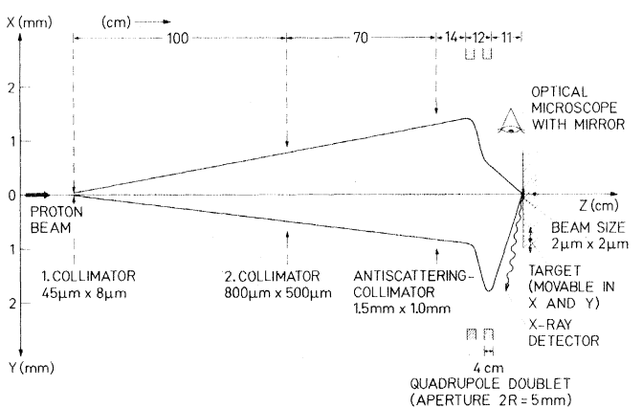

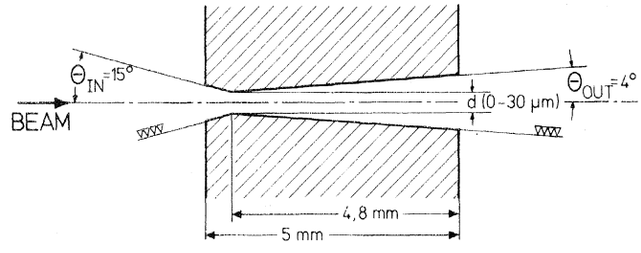

Fig. 2 (left). Schematic view of the proton scanning microprobe. Fig. 3 (right). Side view of the beam-defining edges of the stainless steel collimator slit. The roughness of the surfaces and of the beam-defining edges is ≤ 0.1 μm (triangles).

self-absorption in the sample. The penetration depth of electrons under standard working conditions ranges from 1 to 5 μm, and the electron microprobe excitation geometry is therefore well defined.

In addition, nuclear reactions of the protons in the beam with some target components can produce additional background γ-rays, which might interfere with characteristic x-rays. The energy dependence of nuclear cross sections is usually different from that of atomic cross sections, so that in most cases the proton-induced γ-rays could be identified by varying the proton energy to avoid misinterpretations of x-ray spectra (*9*).

To demonstrate the performance of the proton microprobe, we used it to determine the trace elements in some mineral grains in a lunar basalt (Apollo 17 sample 75015) whose compositions were previously determined with the electron microprobe. Two minerals, ilmenite ($FeTiO_3$) and baddeleyite (ZrO_2), were chosen to look for trace elements which were not detected by the electron microprobe. Two grains of ilmenite and one of baddeleyite were analyzed quantitatively with the electron microprobe, with the results shown in Table 1 (*10*). Qualitative analyses were also carried out at 15 to 30 keV, respectively, using an Si(Li) detector attached to the electron microprobe. No elements other than those measured qualitatively could be detected.

In agreement with the results of previous electron microprobe investigations (*11*), we found that the Zr in Apollo 17 ilmenites is below the detection limit of the electron microprobe. The insets in Figs. 4, 5, and 6 show the electron microprobe spectra of the two ilmenite grains and the baddeleyite measured at an excitation energy of 15 keV. Figure 7 shows the spectra obtained from baddeleyite (Fig. 7a), a zirconolite grain (Ca,Fe)(Zr,Y)Ti_2O_7 attached to baddeleyite (Fig. 7b), and a third ilmenite grain (Fig. 7c) measured with the electron microprobe at 30 keV. In Fig. 7, a and b, the spectra of baddeleyite and zirconolite display the *K* lines of Zr and Y and of Zr, respectively, above 14 keV. None of these lines are visible in the ilmenite spectrum (Fig. 7c).

The two ilmenite grains and the baddeleyite were than analyzed with the proton microprobe at excitation energies of 2 and 4 MeV, with the results shown in Figs. 4, 5, and 6. A typical recording time was 2 hours. The K_α and K_β lines of Y, Zr, and Nb are well developed in the spectra of ilmenite 3 and ilmenite 6, respectively (Figs. 4 and 5). Note the ab-

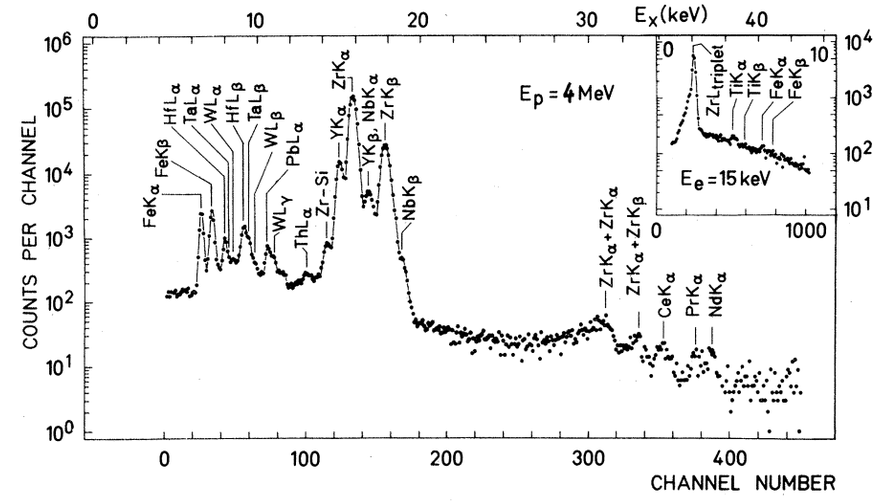

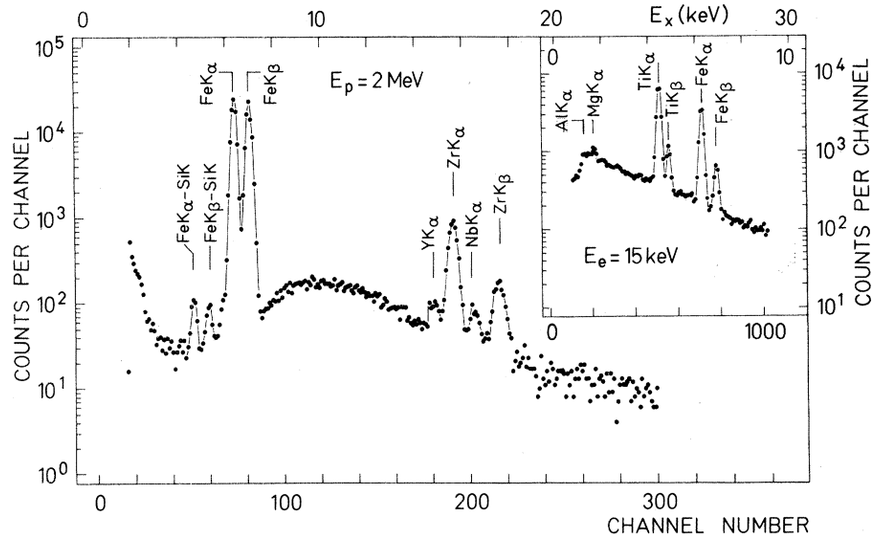

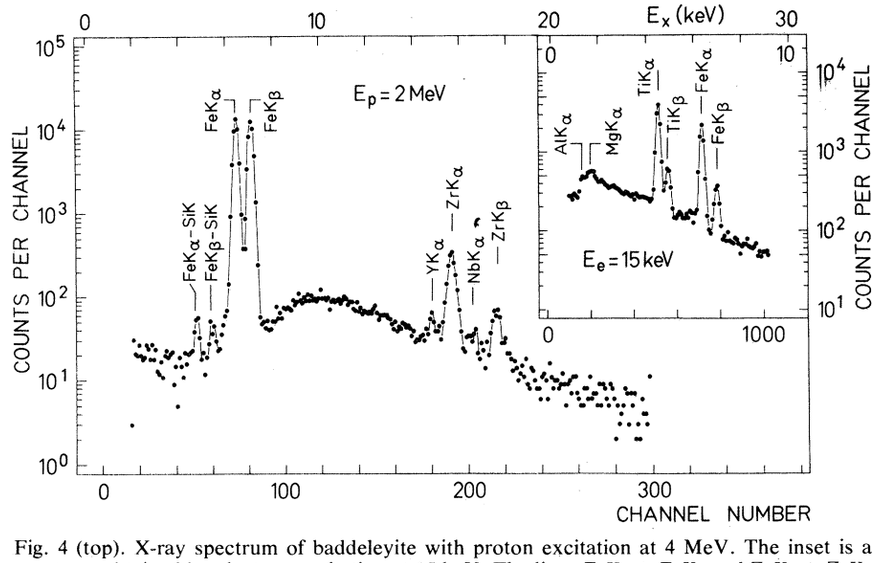

Fig. 4 (top). X-ray spectrum of baddeleyite with proton excitation at 4 MeV. The inset is a spectrum obtained by electron excitation at 15 keV. The lines $ZrK_\alpha + ZrK_\alpha$ and $ZrK_\alpha + ZrK_\beta$ indicate the Zr pile-up peaks. Fig. 5 (middle). X-ray spectrum of ilmenite 3 obtained with proton excitation at 2 MeV. The inset is the spectrum taken with the electron microprobe at 15 keV for the same grain. The *K* spectra of Y, Zr, and Nb are well developed in the proton probe spectrum. Fig. 6 (bottom). X-ray spectrum of ilmenite 6, which is later in the crystallization sequence than ilmenite 3, obtained with proton excitation at 2 MeV. The inset is the spectrum taken with the electron microprobe at 15 keV for the same grain. The *K* spectra of Y, Zr, and Nb are well developed in the proton probe spectrum. The lower intensities of YK_α and NbK_α are noticeable.

sence of the L lines of these elements in the spectra taken at 15 keV because of the high bremsstrahlung background (insets in Figs. 4 and 5). The spectrum of baddeleyite (Fig. 6) revealed the presence of K lines of trace elements which were not detected with the electron microprobe, such as Ta, Pb, Th, W, Y, Nb, Ce, Pr, and Nd. Because of the small grain size of the baddeleyite crystal and its intimate intergrowth with the zirconolite grain, we cannot exclude the possibility that the x-rays of the elements measured by the proton microprobe in the baddeleyite were excited in both baddeleyite and zirconolite. For this reason, we excluded this spectrum from our quantitative evaluation.

For brevity, we give only the concentrations of the lowest three out of the elements detected. The intensities of these K lines (Y, Zr, and Nb) in the spectra of the two ilmenite grains were determined by the following method. The yield of K-hole production for every element was calculated according to the binary encounter approximation (BEA) theory (*8*), taking into account the continuously changing energy of the projectile in the sample. This value was then corrected for fluorescence yield and self-absorption in the target. X-ray absorption in the absorber and the energy-dependent efficiency of the Si(Li) detector were also taken into consideration. The relative mass concentrations were obtained to within a few percent. To obtain absolute values, however, these would have to be referred to a calibrated standard.

In Table 2 we show elements measured with the proton microprobe that were not seen with the electron microprobe. Some calculated mass concentrations referred to the Zr concentration are also given (*10*). The use of Si(Li) solid-state detectors, however, puts some limitations on the applicability of the proton probe, especially in materials containing several 3*d* transition elements as major components. To reduce the total count rates one is forced to use absorbers thick enough to eliminate the majority of the x-ray quanta of the major elements. Thus the x-rays of trace elements with higher energies than those of the major elements may be detected.

In the geological sciences, especially petrology and geochemistry, the technique should allow determination of the partitioning of trace elements among coexisting minerals or phases in natural rocks and multicomponent synthetic material.

The results presented above demonstrate the ability of the proton microprobe to show trace elements in solids that cannot be detected, even qualitatively, with the electron microprobe. The analysis of water-bearing biological samples, however, is not as straightforward as that of solids. Before preparing biological samples for analysis, certain precautions have to be taken. Shock freezing of the specimen is needed to prevent migration of water-soluble ions such as K^+, Na^+, and Cl^- (*12*). Prepared in such a way, the specimen is an excellent insulator. During electron microprobe analysis the electrons will be stopped within the sample, and a strong space charge will be built up in the volume of interest. The electrons will reach the specimen surface with reduced energy, or diffusible ions will be dislocated (*13, 14*). In contrast, protons with energies of, say, 1 MeV will traverse the thin specimen (1 to 10 μm thick). Under these circumstances (i) charging of the specimen is avoided; (ii) the protons lose most of their energy in an electrically conducting backing (such as carbon) and the specimen itself will not be heated; and (iii) protons are more rigid than electrons, so that scattered particles should not increase the volume being examined (*15*).

Table 2. Calculated concentrations of Zr, Y, and Nb as measured with the proton microprobe in ilmenite 3 and ilmenite 6 in lunar sample 75015.

Element	Concentration (ppm) in	
	Ilmenite 3	Ilmenite 6
Zr	1600 ± 300	1000 ± 200
Y	60 ± 20	95 ± 30
Nb	40 ± 15	45 ± 15

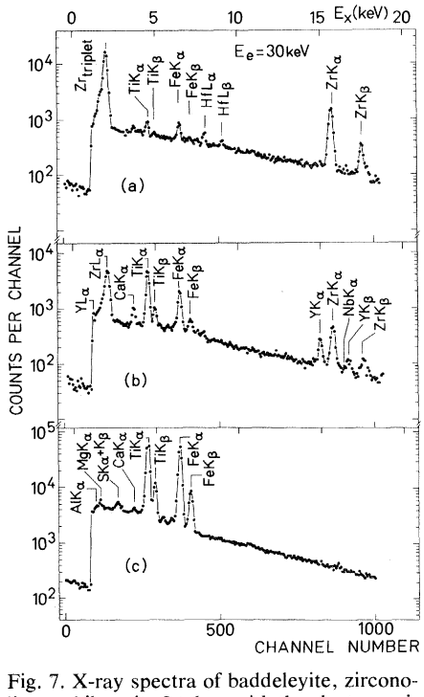

Fig. 7. X-ray spectra of baddeleyite, zirconolite, and ilmenite 3 taken with the electron microprobe at an excitation energy of 30 keV. (a) Spectrum of baddeleyite with a well-developed ZrL triplet and ZrK_α and K_β lines. (b) Spectrum of zirconolite; notice the K spectra of Y and Zr. (c) Spectrum of ilmenite 3. Neither the L nor the K spectra of Y, Zr, and Nb are present. The SK_α and K_β lines at 2.3 and 2.46 keV are excited from a neighboring troilite (FeS) grain.

FRITZ BOSCH
AHMED EL GORESY
BERND MARTIN
BOGDAN POVH
Max-Planck-Institut für Kernphysik, D-6900 Heidelberg, Germany
RAINER NOBILING
DIRK SCHWALM*
KURT TRAXEL
Physikalisches Institut der Universität Heidelberg, D-6900 Heidelberg

References and Notes

1. H. Liebl, *J. Phys. E* **8**, 797 (1975).
2. F. Hillenkamp, E. Unsöld, R. Kaufmann, R. Nitsche, *Appl. Phys.* **8**, 341 (1977).
3. S. A. E. Johansson and T. B. Johansson, *Nucl. Instrum. Methods* **137**, 473 (1976) and references cited therein; Proceedings of the International Conference on PIXE and Its Application, Lund, Sweden, 1977, *ibid.* **142** (1977).
4. R. Nobiling, F. Bosch, Y. Civelekoglu, B. Martin, B. Povh, D. Schwalm, K. Traxel, *ibid.* **142**, 49 (1977).
5. F. Folkmann, *J. Phys. E* **8**, 429 (1975).
6. J. A. Cookson and F. D. Pilling, *Thin Solid Films* **19**, 381 (1973); M. Peisach, D. A. Newton, P. F. Peck, T. B. Pierce, *J. Radioanal. Chem.* **16**, 445 (1973); Z. H. Cho, M. Singh, A. Mohabbatizadeh, *IEEE Trans. Nucl. Sci.* **NS-21**, 622 (1974).
7. R. Nobiling, Y. Civelekoglu, B. Povh, D. Schwalm, K. Traxel, *Nucl. Instrum. Methods* **130**, 325 (1975).
8. J. D. Garcia, R. J. Fortner, T. M. Kavanagh, *Rev. Mod. Phys.* **45**, 111 (1974).
9. F. Bosch, A. El Goresy, W. Krätschmer, B. Martin, R. Nobiling, B. Povh, D. Schwalm, K. Traxel, *Z. Phys. A* **280**, 39 (1977); *Phys. Rev. Lett.* **37**, 1515 (1976).
10. Matrix corrections were performed using the automation program "Geolab" with the correction factors of Albee and Ray (*14*).
11. A. El Goresy, P. Ramdohr, O. Medenbach, H.-J. Bernhardt, in *Proceedings of the Fifth Lunar Science Conference*, W. A. Gose, Ed. (Pergamon, New York, 1974), suppl. 5, vol. 1, p. 627.
12. W. Fuchs and B. Lindemann, *J. Microsc.* **22**, 227 (1975).
13. M. P. Borom and R. E. Hannemann, *J. Appl. Phys.* **38**, 2406 (1967).
14. A. L. Albee and L. Ray, *Anal. Chem.* **42**, 1408 (1970).
15. We have explored, in collaboration with Dr. Petzelt, Deutsches Krebsforschungszentrum, Heidelberg, the applicability of the proton microprobe to biological objects with sizes of the order of 10 μm. Investigating a dehydrated sea urchin egg 40 μm in diameter in a first test, we were able to analyze the changes of the Ca/S ratio in 12 points along the scanning line. The spatial resolution was about 2 μm. As the measured values are fully reproducible, we suppose that we can also perform a differential trace element analysis, for example, of human cells.

16. We are grateful to the workshop of the Physikalisches Institut der Universität Heidelberg, especially to E. Ehrbar, for the excellent machining of the microprobe facility. The help of H. Döbbeling and J. Sarbin during the experiment and the support of the drafting bureau of the Max-Planck-Institut für Kernphysik, Heidelberg, are acknowledged.

* Present address: Gesellschaft für Schwerionenforschung mbH, P.O. Box 541, D-6100 Darmstadt, Germany.

23 May 1977; revised 12 December 1977